
Calibrated Test-Time Guidance for Bayesian Inference

Daniel Geyman^{*1} Felix Draxler^{*1} Jan Groeneveld¹ Hyunsoo Lee² Theofanis Karaletsos³ Stephan Mandt¹

Abstract

Test-time guidance is a widely used mechanism for steering pretrained diffusion models toward outcomes specified by a reward function. Existing approaches, however, focus on maximizing reward rather than sampling from the true Bayesian posterior, leading to miscalibrated inference. In this work, we show that common test-time guidance methods do not recover the correct posterior distribution and identify the structural approximations responsible for this failure. We then propose consistent alternative estimators that enable calibrated sampling from the Bayesian posterior. We significantly outperform previous methods on a set of Bayesian inference tasks, and match state-of-the-art in black hole image reconstruction.

1. Introduction

Diffusion models (Sohl-Dickstein et al., 2015; Song & Ermon, 2019; Ho et al., 2020; Song et al., 2021) and their flow matching variants (Liu et al., 2023; Lipman et al., 2023; Albergo & Vanden-Eijnden, 2023) have achieved tremendous success in sampling high-quality yet diverse natural images (Dhariwal & Nichol, 2021; Rombach et al., 2022) and videos (Yang et al., 2023; Ho et al., 2022) as well as scientific applications such as molecule generation (Hoogeboom et al., 2022) and protein-ligand docking (Corso et al., 2023).

A core advantage of diffusion models over competing generative models is their ability to sample from tilted distributions at test time: Take a pretrained model and guide the generation towards a desired outcome as specified by a potentially nonlinear reward function (Chung et al., 2023). This enables applying pretrained diffusion models to inverse problems such as super-resolution, deblurring, denoising, style guidance, image editing, and more without any addi-

tional training.

This approach is motivated by the goal of sampling from the Bayesian posterior, proportional to the diffusion model prior and a likelihood function that specifies the task (often called reward). In this work, we find that **existing test-time adaptation methods do not actually sample from the Bayesian posterior**, see Figure 1. Instead, they sample from biased distributions. We attribute this bias to the common approximations of the expected reward function in a noisy diffusion state, as well as to an overly simple usage of guidance scales.

We contribute:

- We find that existing test-time guidance methods do not sample from the true Bayesian posterior (Section 4). We prove that they use biased estimators for the diffused likelihood regardless of the task (Theorems 4.1 to 4.3), suggesting why they do not converge to the true posterior even with more compute.
- We propose Calibrated Bayesian Guidance (CBG), a new consistent yet tractable guidance framework that leads to sampling the correct diffusion posterior in Section 5. Our framework supports non-differentiable objectives.
- Experimentally, our estimators accurately approximate the Bayesian posterior on a variety of inverse problems and match state-of-the-art PSNR on a black-hole imaging task.

Together, we illustrate and address an important gap in the literature to accurately sample from Bayesian posteriors based on pretrained diffusion model priors.

2. Background

2.1. Diffusion Models

Diffusion models represent a data distribution $p(x)$ by iteratively transforming samples from a latent distribution $p(x_1)$ (usually a standard normal) through a stochastic or ordinary differential equation parameterized by a neural network $s_\theta(x_t, t)$ towards data samples of $p_\theta(x)$. The idea is to learn a neural network to reverse the addition of noise to

¹Department of Computer Science, University of California, Irvine, CA, USA ²Seoul National University, Seoul, South Korea ³Chan-Zuckerberg Initiative, Redwood City, CA, USA. Correspondence to: Felix Draxler <fdraxler@uci.edu>, Stephan Mandt <mandt@uci.edu>.

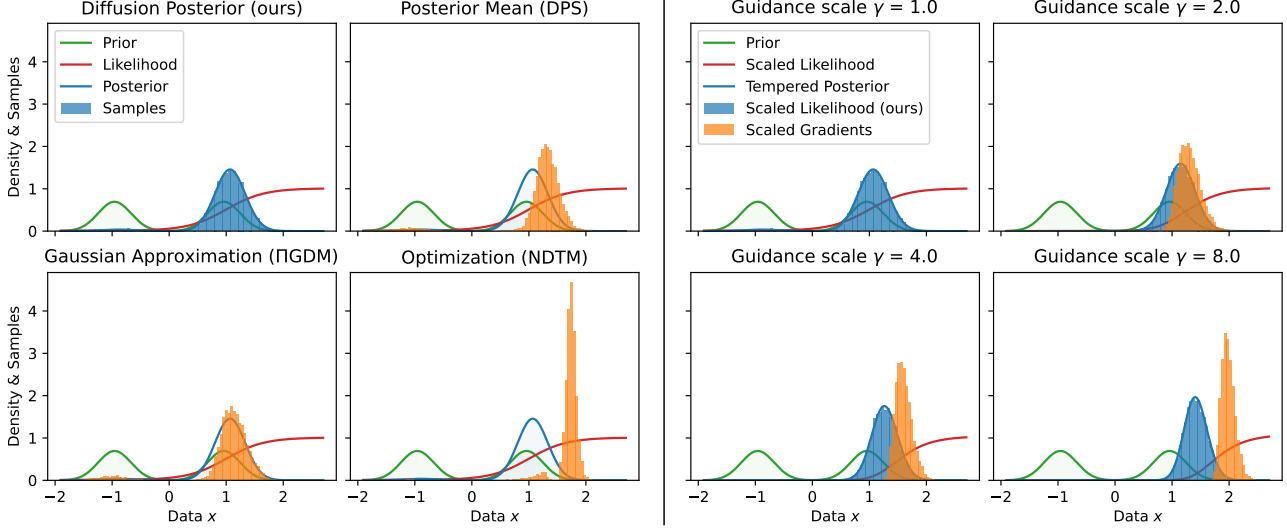


Figure 1. We present a test-time guidance scheme to sample from calibrated Bayesian posteriors. (Left) Our framework accurately samples the correct posterior (blue). Posterior mean (Equation (7)), posterior Gaussian (Equation (8)), and optimal control approximations (Equation (9)) to the diffused likelihood $p(y | x_t)$ yield uncalibrated samples (orange). (Right) Our framework can correctly sample from tempered posteriors $p(x | y, \gamma) \propto p(x)p(y | x)^\gamma$ (blue). Rescaling the noisy gradient by γ leads to biased samples, even if the diffused likelihood $p(y | x_t)$ is accurately estimated (orange).

the training data $x \sim p(x)$:

$$p(x_t | x) = \mathcal{N}(x_t; a_t x, b_t^2 I). \quad (1)$$

We adopt the convention that $t = 0$ corresponds to the data distribution (so $a_0 = 1$ and $b_0 = 0$), and $t = 1$ is the noisy latent ($a_1 = 0$ and $b_1 = 1$). We write $x = x_0$ for noise-free data samples.

The ordinary differential equation for sampling from a diffusion model is given by (Karras et al., 2022):

$$\frac{dx}{dt} = \frac{\dot{a}_t}{a_t} x - b_t^2 \dot{a}_t a_t \underbrace{\nabla_{x_t} \log p(x_t)}_{\text{learned } s_\theta(x_t, t)}. \quad (2)$$

Diffusion models are learned by minimizing the following loss:

$$\mathbb{E}_{t \sim \mathcal{U}[0, 1], x \sim p(x), x_t \sim p(x_t | x)} \left[\left\| \frac{a_t x - x_t}{b_t^2} - s_\theta(x_t, t) \right\|^2 \right]. \quad (3)$$

Other formulations of diffusion rewrite Equation (3) to instead predict the mean $f_\theta(x_t, t) \approx \mathbb{E}[x | x_t]$ or the instantaneous velocity $v_\theta(x_t, t) \approx \mathbb{E}_{x|x_t}[x - \epsilon | x_t]$, where $x_t = a_t x + b_t \epsilon$. They also introduce weighting functions $\lambda(t)$ that rescale the loss for better convergence, or sample $t \sim p(t)$. Similarly, different choices for the coefficients a_t, b_t lead to different formulations of diffusion and flow matching.

For the experiments in this paper, we choose the schedules ourselves, or leverage pretrained models, in which case we adopt their diffusion schedule.

2.2. Bayesian inference

We are interested in sampling from the Bayesian posterior:

$$p(x | y) \propto p(x)p(y | x). \quad (4)$$

Here, the prior $p(x)$ is usually given by training a diffusion model on data; in our experiments in Section 6.1, we find that it is even useful for analytic priors with tractable noising convolutions. The ‘‘observation’’ y is an abstract placeholder for specifying the task: It could be a noisy measurement, but also covers arbitrary reward functions $r(x; y)$, potentially without an external signal $r(x; y) \equiv r(x)$, so that $p(y | x) = \exp(r(x; y))$.

Sampling from Equation (4) is a hard task in general. Diffusion models can be used here by learning them as a prior distribution $p(x)$. The core insight is that given a pretrained diffusion model, we can modify its prediction to correct from the diffusion prior to the Bayesian posterior via Bayes’ rule:

$$\nabla_{x_t} \log p(x_t | y) = \underbrace{\nabla_{x_t} \log p(x_t)}_{\text{pretrained model}} + \underbrace{\nabla_{x_t} \log p(y | x_t)}_{\text{diffused likelihood}}. \quad (5)$$

While this modification is formally correct, the general form of the likelihood $p(y | x)$ in Equation (4) makes it impossible to analytically compute the diffused likelihood $p(y | x_t)$ on noisy data as required for Equation (5), even if we have a closed-form expression for $p(y | x)$.

Instead, we need to approximate this integral, which evalu-

ates to:

$$p(y | x_t) = \int p(x | x_t)p(y | x)dx, \quad (6)$$

where $p(x | x_t)$ samples from the diffusion denoising posterior.

The central goal of this paper is to identify valid approximations of the integral in Equation (6) that lead to sampling from the true Bayesian posterior $p(x | y)$ as defined in Equation (4).

2.3. Diffused likelihood approximation

Equation (6) is usually approximated to save costs. In this section, we show how these approximations prevent sampling from the correct posterior.

The common approximations in the literature are:

- The **Posterior Mean Approximation** computes the cost of the mean, instead of the mean of the cost (Chung et al., 2023):

$$p(y | x_t) \approx p(y | x = \mathbb{E}[x | x_t]). \quad (7)$$

Intuitively, this is justified late in sampling when the diffusion posterior has small support relative to the curvature of the reward.

- Evaluate Equation (6) with a **Posterior Gaussian Approximation** to the denoising distribution $p(x | x_t)$, as proposed as IIGDM (Song et al., 2023a):

$$p(y | x_t) \approx \int p(y | x)\mathcal{N}(x; \mathbb{E}[x | x_t], \sigma_t^2 I)dx. \quad (8)$$

The standard deviation is typically chosen as $\sigma_t^2 = b_t^2/(a_t^2 + b_t^2)$, the correct value if the prior $p(x)$ is a standard normal distribution.

- **Optimal control** formulations such as nonlinear diffusion trajectory matching (NDTM) (Pandey et al., 2025b) steer the trajectory through a local optimization problem:

$$\tilde{x}_t = x_t + u_t, \text{ where } u_t = \operatorname{argmin}_{u_t} \mathcal{L}(u_t, x_t) \quad (9)$$

The loss function $\mathcal{L}(u_t, x_t)$ usually regularizes finite control u_t plus maximizes the posterior mean approximation in Equation (7). The optimization over u_t broadens the design space of the guidance framework. While this usually leads to higher rewards, it does not aim for calibrated posterior sampling.

We analyze the shortcomings of these estimators in Section 4 and propose a well-calibrated alternative in Section 5.

3. Related Work

Our training-free guidance framework is based on diffusion models. Diffusion models learn to generate data by iteratively denoising samples from a simple noise distribution, with foundational formulations ranging from discrete-time diffusion processes (Sohl-Dickstein et al., 2015; Ho et al., 2020) to continuous-time and score-based (Song & Ermon, 2019; Song et al., 2021) as well as velocity-based perspectives (Liu et al., 2023; Lipman et al., 2023; Albergo & Vanden-Eijnden, 2023). These methods have demonstrated strong empirical performance across modalities by training neural networks to approximate the reverse diffusion dynamics. Regarding the calibration of these models, existing work analyzes epistemic uncertainty (Jazbec et al., 2025), and improves tail behavior (Pandey et al., 2025a).

The test-time guidance framework we develop in this paper leverages pretrained diffusion models and adapts them to novel tasks. The first approaches to solving inverse problems using diffusion models consider *linear* tasks such as inpainting, super-resolution, and colorization (Kadkhodaie & Simoncelli, 2021; Song et al., 2021; Chung et al., 2022b; Kawar et al., 2022; Chung et al., 2022a). The methods developed for linear tasks make tailored changes to the diffusion sampling to adhere to the task specification, not aiming to recover the Bayesian posterior.

Diffusion Posterior Sampling (DPS) (Chung et al., 2023) generalized this to solve nonlinear inverse problems using the posterior mean approximation. Several follow-up works extend DPS to more tasks, such as Universal Guidance for Diffusion Models (Bansal et al., 2024) and FreeDoM (Yu et al., 2023). We find that the posterior mean approximation can yield high adherence to the reward, but that the samples do not follow the Bayesian posterior.

To combat the inaccuracies in the posterior mean approximation, Pseudoinverse-Guided Diffusion Models (IIGDM) (Song et al., 2023a) and C-IIGDM (Pandey et al., 2024) approximate the diffusion posterior $p(x | x_t)$ by a normal distribution around Tweedie’s estimate. This approximation is also used in Loss-Guided Diffusion (LGD) (Song et al., 2023b) as well as Diffusion Policy Gradient (DPG) (Tang et al., 2023).

MPGD (He et al., 2024) project the posterior mean to the data manifold and evaluate the likelihood there. This alleviates the problem that the reward function might be ill-defined off the data manifold, a common scenario for posterior approximations. However, this method is still limited by a single point estimate for the diffusion posterior.

Unified Training-Free Guidance (TFG) (Ye et al., 2024) unify several design decisions underlying previous methods. Similarly, Nonlinear Diffusion Trajectory Matching (NDTM) (Pandey et al., 2025b) extend the design

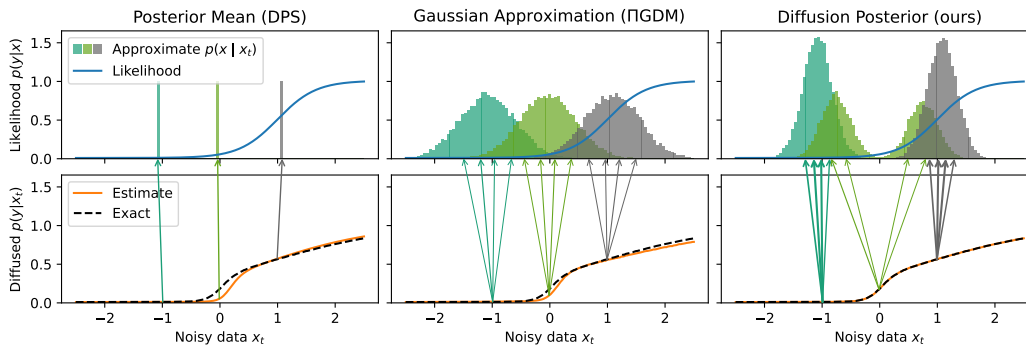


Figure 2. **Approximations of diffused likelihoods.** (Left) The posterior mean approximation in Equation (7) looks up the likelihood value at the mean of the diffusion posterior. (Center) Gaussian approximations to the posterior lead to inconsistent estimates that cannot be corrected by sampling more points. (Right) Our method relies on the true diffusion posterior $p(x_t | x)$, yielding arbitrary precision to determine the diffused likelihood $p(y | x_t)$ and its gradients.

space, but ultimately both rely on the posterior mean approximation. Divide-and-Conquer Posterior Sampling (DCPS) (Janati et al., 2024) perform local Monte Carlo updates at every diffusion step.

In contrast to all these works, we formulate a consistent diffusion posterior sampling, where increased computational budget leads to calibrated samples. In concurrent work, Potapchik et al. (2026) train few-step models to evaluate the same estimators as in Equations (16) and (20). While the focus of that work is on image synthesis, we focus on Bayesian inference.

A complementary body of work proposes to learn the diffused likelihood directly, which requires retraining for new tasks. This is achieved in classifier-free guidance (Ho & Salimans, 2021), which requires the likelihood to be representable as an input to the model. Other methods leverage reinforcement learning techniques to learn the diffused likelihood or finetune the teacher to a given reward (Li et al., 2024; Fan et al., 2023; Black et al., 2024; Uehara et al., 2024).

4. Shortcomings of Existing Estimators

We now derive that the approximations of the diffused likelihoods in Section 2.3 yield uncalibrated Bayesian posteriors. In particular, we show that the approximations are always biased, apart from trivial cases.

4.1. Inconsistency of Diffused Likelihood Estimators

The estimators introduced in Equations (7) to (9) in Section 2.3 have one common pitfall: They are inconsistent estimators, meaning that even increasing the computational budget will not approximate the true diffused likelihood in Equation (6). Instead, they converge to a biased estimate.

First, we characterize that the posterior mean approximation

in Equation (7) is always biased, unless the likelihood is constant, which corresponds to sampling from the prior:

Theorem 4.1. *Given a prior $p(x)$ that is Lipschitz and a twice differentiable likelihood $p(y | x)$: The posterior mean approximation in Equation (7) is biased for some $0 < t < 1$ unless the likelihood $p(y | x)$ is constant in x .*

The Lipschitz assumption imposes no practical restriction; it means that the data distribution cannot have infinite jumps. Both the proof of the theorem and a discussion of its practical relevance are given in Section A.1.

Similarly, the Gaussian posterior approximation is only correct if the likelihood is trivial or the prior $p(x)$ is a standard normal:

Theorem 4.2. *Given a prior $p(x) \neq \mathcal{N}(x; 0, I)$ and a likelihood $p(y | x)$: The Gaussian posterior approximation for $p(y | x_t)$ in Equation (8) is biased for every $0 < t < 1$ unless $p(y | x)$ is constant in x .*

Please see Section A.2 for a detailed proof.

Figure 1 (left) shows how this leads to methods relying on these estimates to sample from incorrect posteriors: Every step in the guided diffusion process in Equation (5) follows an approximation of the guidance term that ultimately leads to bad calibration. Figure 2 visualizes how the different approaches approximate the diffused likelihoods.

In Section 5, we will derive novel estimators for the diffused likelihoods that are consistent: Increasing the computational budget for the diffused likelihood makes the estimator converge to the true value.

4.2. Bias of Guidance Scales

However, even if we have access to a correct $p(y | x_t)$, there is another common bias introduced when guiding diffusion models: It occurs when one tries to vary the importance of the prior $p(x)$ relative to the likelihood $p(y | x)$ using a

parameter γ :

$$p(x | y, \gamma) \stackrel{\text{def}}{\propto} p(x)p(y | x)^\gamma. \quad (10)$$

This is referred to as a tempered likelihood posterior in Bayesian inference (Wuttke et al., 2014; Mandt et al., 2016; Friel & Pettitt, 2008; Pawlowski et al., 2017).

In the context of diffusion models, γ is referred to as the classifier or the guidance scale (Ho & Salimans, 2021; Dhariwal & Nichol, 2021). It is usually implemented by rescaling the likelihood term in Equation (5):

$$\nabla_{x_t} \log p(x_t) + \gamma \nabla_{x_t} \log p(y | x_t). \quad (11)$$

Assume now that we have access to the ground truth $p(y | x_t)$ for $\gamma = 1$. Equation (11) would imply that the *tempered* diffused likelihood reads:

$$p(y | x_t, \gamma) \stackrel{?}{=} p(y | x_t)^\gamma. \quad (12)$$

However, this is not correct. According to the definition in Equation (6), the guidance scale needs to be applied *within the integral*:

$$p(y | x_t, \gamma) \propto \int p(x | x_t)p(y | x)^\gamma dx. \quad (13)$$

In fact, we can show that Equation (12) is only correct in the trivial case where the likelihood is constant, in which case guidance has no effect:

Theorem 4.3. *For all $1 > t > 0$ and $\gamma \in \mathbb{R}_+ \setminus \{0, 1\}$: The tempered diffused likelihood cannot be obtained through exponentiation: $p(y | x_t, \gamma) \neq p(y | x_t)^\gamma$ unless $p(y | x)$ is constant with respect to x .*

The proof is given in Section A.3.

So whenever the likelihood is of any interest at all, picking Equation (12) instead of Equation (13) results in an error. Figure 1 (right) shows how the incorrect Equation (11) as opposed to the correct Equation (13) leads to sampling from an incorrect tempered posterior.

Notably, this restriction not only applies to existing test-time guidance methods, but it also applies to classifier guidance (Ho & Salimans, 2021), for which we can only extract the untempered diffused likelihood gradient:

$$\nabla_{x_t} \log p(y | x_t) \approx \nabla_{x_t} \log p_\theta(x_t | y) - \nabla_{x_t} \log p_\theta(x_t). \quad (14)$$

Only a tempered conditional model $p_\theta(x_t | y, \gamma)$ can extract the correct tempered diffused likelihood gradient.

This means rescaling the diffused likelihood gradient is not enough for calibrated tempered inference.

Together, these results imply that no amount of additional computation can correct the bias in existing methods: they

converge to the wrong distribution. We now derive a consistent test-time guidance framework that is immune to the shortcomings in Sections 4.1 and 4.2.

5. Calibrated Bayesian Guidance (CBG)

In the light of the shortcomings of existing estimators in Section 4, we now present a novel guidance framework that enables consistent sampling from the true Bayesian posterior, both with and without tempering the likelihood. The central idea is to directly approximate the integral in Equation (6).

5.1. Differentiable Rewards

Assuming $p(y | x)$ is differentiable everywhere, we can compute the gradient of the diffused likelihood using the reparameterization trick:

$$\begin{aligned} & \nabla_{x_t} \log p(y | x_t) \\ &= \frac{1}{p(y | x_t)} \nabla_{x_t} \int p(x | x_t)p(y | x) dx \\ &= \frac{1}{p(y | x_t)} \nabla_{x_t} \int p(y | x = g_t(x_t; \epsilon))p(\epsilon) d\epsilon \\ &= \frac{1}{p(y | x_t)} \int \nabla_{x_t} p(y | x = g_t(x_t; \epsilon))p(\epsilon) d\epsilon. \end{aligned} \quad (15)$$

Here, $g_t(x_t; \epsilon)$ samples from $p(x | x_t)$ such that it is differentiable with respect to x_t , and ϵ is the randomness that is used to sample from it.

This makes the gradient of the diffused likelihood straightforward to estimate:

$$\begin{aligned} & \nabla_{x_t} \log p(y | x_t) \\ & \approx \frac{1}{\sum_i p(y | x^{(i)})} \sum_{i=1}^K \nabla_{x_t} p(y | x = g(x_t; \epsilon^{(i)})). \end{aligned} \quad (16)$$

Here, $\epsilon^{(i)} \sim p(\epsilon)$ samples the randomness in the sampler g for samples $i = 1, \dots, K$. For example, DDPM (Ho et al., 2020) can be used to sample from $x \sim p(x | x_t)$. Then, $\epsilon^{(i)}$ collects the noise added in all diffusion steps in order to get the sample $x^{(i)}$. We call Equation (16) **Gradient-Based Calibrated Bayesian Guidance**.

In practice, we work with log-likelihoods $\log p(y | x)$ and average using $\text{softmax}(w_i)$ for numeric stability.

Equation (16) yields a consistent sampling procedure: as $K \rightarrow \infty$, any bias vanishes. This stands in contrast to the estimators considered in Section 2.3, which remain biased even asymptotically. While consistency requires averaging over multiple samples to obtain a reliable guidance signal, the additional computation can be viewed as the necessary cost of eliminating systematic bias rather than a fundamental limitation of the estimator itself.

5.2. Non-differentiable Rewards

The reparameterization estimator Equation (16) has the major drawback that it is not compatible when computing gradients through the sampling process $p(x | x_t)$ and/or the likelihood $p(y | x)$ is computationally expensive or intractable.

To this end, we propose a REINFORCE estimator (Williams, 1992) to compute the gradient of the diffused likelihood in Equation (5):

$$\begin{aligned} \nabla_{x_t} \log p(y | x_t) &= \frac{1}{p(y | x_t)} \nabla_{x_t} \int p(x | x_t) p(y | x) dx \\ &= \frac{1}{p(y | x_t)} \int p(x | x_t) p(y | x) \nabla_{x_t} \log p(x | x_t) dx. \end{aligned} \quad (17)$$

Inserting into Equation (5), we absorb $\nabla_{x_t} \log p(x_t)$ into the integral and find for the diffused posterior score:

$$\begin{aligned} \nabla_{x_t} \log p(x_t | y) &= \frac{1}{p(y | x_t)} \int p(x | x_t) p(y | x) \nabla_{x_t} \log p(x_t | x) dx. \end{aligned} \quad (18)$$

By Equation (1), we can replace

$$\nabla_{x_t} \log p(x_t | x) = \frac{a_t x - x_t}{b_t^2}. \quad (19)$$

Evaluated using a finite set of samples $x^{(i)} \sim p(x | x_t)$ for $i = 1, \dots, K$, we find our estimator:

$$\nabla_{x_t} \log p(x_t | y) \approx \frac{1}{\sum_i w_i} \sum_{i=1}^K w_i \frac{a_t x^{(i)} - x_t}{b_t^2}. \quad (20)$$

The likelihood enters as weights $w_i = p(y | x^{(i)})$. We call Equation (20) **Gradient-Free Calibrated Bayesian Guidance**.

Equation (20) is again a consistent estimator, meaning that it is unbiased for a sufficiently large number of samples. Again, the diffusion samples $x^{(i)} \sim p(x | x_t)$ can be obtained using diffusion sampling algorithms.

5.3. Comparing gradient-free and gradient-based methods

One might think that being based on REINFORCE, the gradient-free estimator in Equation (20) has larger variance than the gradient-based estimator in Equation (16), as discussed in (Paisley et al., 2012; Ruiz et al., 2016; Miller et al., 2017).

Interestingly, this general rule does not apply for our estimators, since they involve a self-normalization term of dividing

by the sum of the weights. Empirically, we find that the variance of the gradient-free estimator in Equation (20) is in general lower than that of the gradient-based estimator in Equation (16). See Appendix C for a concrete example.

The reason is that the two estimators behave quite differently in the presence of sharp likelihoods: The gradient-based estimator reduces to a weighted sum, as can be seen by extracting Tweedie’s estimate from Equation (20):

$$\mathbb{E}[x | y] \approx \sum_i \frac{w_i}{\sum_j w_j} x^{(i)}. \quad (21)$$

As the weights w_i are typically of different orders of magnitude in practice, it often considers only the handful of samples with relatively high likelihood. The diffusion process will then move towards these samples in a region of high likelihood, discarding the others.

For the gradient-based estimator in Equation (16), the estimate is dominated by gradients associated with the highest-likelihood samples. These gradients can still be large, since small gradients occur only in a narrow neighborhood around the likelihood maximizer. Moreover, they are effectively amplified because the normalization term is determined by weights that are smaller than the (unobserved) maximum likelihood value:

$$\nabla_{x_t} \log p(y | x_t) \approx \sum_i \frac{\nabla_{x_t} w_i}{\sum_j w_j} \quad (22)$$

As a consequence, a large gradient can induce a disproportionately large update. Reducing this effect requires a larger number of samples, so that local gradients average out into a stable global direction and the maximum observed weight becomes a less noisy estimate of the true tail behavior.

From a practical perspective, the reparameterization estimator also requires computing gradients through the diffusion sampling, which increases computational cost and increases memory consumption. We therefore do not consider it for high-dimensional experiments.

6. Experiments

We now confirm the quality of our framework for practical Bayesian inference tasks. We find that CBG outperforms other test-time guidance method on tasks where the prior and the likelihood are given as closed-form expressions, as well as on a scientific inverse problem where the prior is given by a pretrained diffusion model of black hole images.

6.1. Bayesian Inference Benchmark

In this experiment, we evaluate a diverse collection of diffusion guidance methods on a benchmark of Bayesian inverse problems proposed by Lueckmann et al. (2021). This benchmark is designed to test methods on their distributional fit

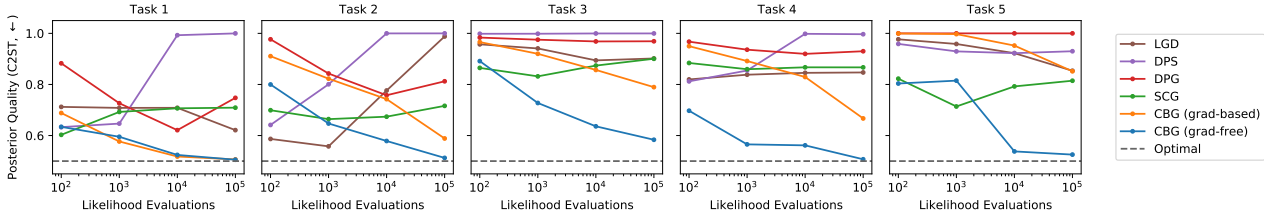


Figure 3. Empirical performance on Bayesian Inference tasks. Performance is measured in C2ST (lower is better, \downarrow) (Friedman, 2004), comparing the distribution of guided samples to those of ground truth samples. Our methods improve performance with more compute, while other test-time adaptation methods are limited due to their approximations to diffused likelihood gradients.

of the true Bayesian posterior $p(x | y)$ at varying computational budgets. To this end, the benchmark provides reference samples from the true posterior.

For the diffusion posterior $p(x | x_t)$ in Equations (16) and (20) as well as for the posterior mean $\mathbb{E}[x | x_t]$ in Equations (7) and (8), we leverage closed-form expressions from the true prior $p(x)$ of these tasks (see Appendix E). This is possible because the prior distributions are not learned, but standard distributions such as normal and uniform. This makes the experiments blazingly fast: A single inference takes on the order of milliseconds.

Figure 3 shows how both our gradient-free and gradient-based estimators improve their C2ST towards the optimal value of 0.5 as the compute budget is increased. Other test-time guidance methods generally do not improve performance with more compute, and converge to a suboptimal distribution.

Additionally, Table 1 shows the best classifier score for each method over all hyperparameters. The gradient-free method achieves the best distributional fit for every task by far compared to all other test-time guidance methods. We also evaluate against a collection of likelihood-free methods that rely only on samples $y^{(i)} | x$ and a target y , instead of an exact likelihood $p(y | x)$. Our CBG method also outperforms these likelihood-free methods on average.

Together, we see that our estimators perform well on Bayesian inverse tasks, and outperform a significant collection of likelihood-based and likelihood-free methods.

6.2. Black Hole Imaging

In this experiment, we evaluate CBG on the black hole imaging task proposed by Zheng et al. (2025), on a diffusion model trained on black hole images by (Mizuno, 2022). This task is designed to evaluate different guidance methods in a standardized way.

This task was chosen because having a calibrated estimator is especially valuable for scientific data and imaging applications. In the domain of natural images, the generation of visually pleasing results that score high in likelihood

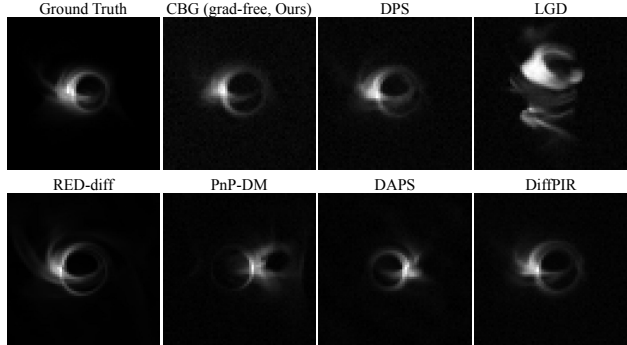


Figure 4. Uncurated comparison of the proposed method with other test-time guidance methods on black-hole imaging task proposed by Mizuno (2022). Despite computing no likelihood gradient, CBG is able to reconstruct the ground truth samples well.

is often the primary goal, while distributional aspects like compliance with the true posterior are secondary.

In particular, it provides an unconditional diffusion model which acts as the prior $p(x)$ as well as 100 samples consisting of a reference solution as well as a corresponding radio-telescope measurement. The likelihood function $p(y | x)$ measures the compatibility of an image x with a given observation y .

We use the gradient-free estimator for our method, as we find the gradient-based estimator to require many samples for good convergence. Given the diffusion prior $p(x)$, we use two nested loops to generate one image. With a diffusion model that is trained for N denoising steps, the outer loop calculates the gradient-free estimator for each timestep $0 \leq t < N$ to run the guided denoising process, while the inner loop needs to calculate $p(x_{0,i} | t_i)$ for each sample i ($1 \leq i \leq K$), where K is a tunable hyperparameter denoting the total number of samples. A vanilla implementation of this algorithm requires $\mathcal{O}(N^2)$ steps. To shorten the runtime, it is enough to use a small number of diffusion steps M ($M < N$) in the inner loop, evenly spaced across the remaining steps, resulting in an overall cost of $\mathcal{O}(NM)$. This way, the inner loop gives a broad estimate in the beginning (sufficient for determining the broad direction), and

Calibrated Test-Time Guidance for Bayesian Inference

Table 1. Best Method Performance on Bayesian Inference C2ST (\downarrow), standard deviations in parentheses.

Algorithm	Task 1	Task 2	Task 3	Task 4	Task 5	Average
<i>Diffusion Methods</i>						
CBG (gradient-free, ours)	0.505 (0.004)	0.513 (0.009)	0.584 (0.063)	0.507 (0.006)	0.525 (0.028)	0.527
CBG (gradient-based, ours)	0.507 (0.005)	0.589 (0.048)	0.789 (0.089)	0.667 (0.019)	0.852 (0.038)	0.681
DPS (Chung et al., 2023)	0.633 (0.024)	0.641 (0.032)	0.998 (0.002)	0.812 (0.023)	0.929 (0.045)	0.803
LGD (Song et al., 2023b)	0.621 (0.049)	0.558 (0.013)	0.894 (0.042)	0.820 (0.028)	0.854 (0.117)	0.750
DPG (Tang et al., 2023)	0.621 (0.078)	0.758 (0.027)	0.968 (0.015)	0.920 (0.023)	1.000 (0.000)	0.872
SCG (Huang et al., 2024)	0.603 (0.037)	0.664 (0.028)	0.832 (0.027)	0.860 (0.017)	0.714 (0.131)	0.735
<i>Likelihood-free Methods</i>						
NLE (Papamakarios et al., 2019)	0.515 (0.009)	0.506 (0.004)	0.699 (0.069)	0.731 (0.023)	0.668 (0.094)	0.624
NPE (Papamakarios & Murray, 2016)	0.506 (0.004)	0.509 (0.005)	0.831 (0.052)	0.555 (0.015)	0.542 (0.024)	0.589
NRE (Hermans et al., 2020)	0.536 (0.031)	0.631 (0.034)	0.919 (0.039)	0.734 (0.019)	0.629 (0.056)	0.690
REJ-ABC (Pritchard et al., 1999)	0.802 (0.023)	0.909 (0.028)	0.961 (0.020)	0.772 (0.034)	0.664 (0.040)	0.822
SMC-ABC (Beaumont et al., 2009)	0.726 (0.032)	0.794 (0.041)	0.963 (0.018)	0.664 (0.011)	0.663 (0.048)	0.762
SNLE (Papamakarios et al., 2019)	0.519 (0.008)	0.509 (0.005)	0.578 (0.029)	0.624 (0.089)	0.571 (0.050)	0.560
SNPE (Greenberg et al., 2019)	0.507 (0.004)	0.507 (0.005)	0.666 (0.061)	0.533 (0.014)	0.530 (0.026)	0.545
SNRE (Hermans et al., 2020)	0.515 (0.004)	0.536 (0.007)	0.721 (0.058)	0.542 (0.016)	0.563 (0.032)	0.575

better estimates later (good to get a clean image) because the individual diffusion steps get smaller. Because the estimator is consistent, results improve with higher K and M . For our experiments, we selected $K = 512$ and $M = 50$ as a trade-off between computational effort and image results.

We compare the proposed method against two categories of baselines obtained from (Zheng et al., 2025). First, we include traditional image reconstruction methods such as Chandra et al. (2018); Chael et al. (2018). Second, we compare with recent test-time guidance approaches (Chung et al., 2023; Song et al., 2023b; Mardani et al., 2024; Wu et al., 2024; Zhang et al., 2024; Zhu et al., 2023), which incorporate diffusion models as implicit priors for solving inverse problems. All test-time guidance methods are evaluated using the implementation provided by (Zheng et al., 2025), following the same experimental protocol for fair comparison.

Figure 4 visualizes uncurated qualitative reconstruction results. While some of the baselines produce results that are either noticeably blurred or fail to faithfully follow the ground-truth, our method yields results that are visually consistent with the ground truth.

Table 2 shows that our method matches the state-of-the-art in terms of peak signal-to-noise ratio (PSNR, higher is better). It measures the pixel-wise similarity between a reconstructed image and the ground truth, expressed in decibels, and thereby directly quantifies how close the reconstruction is to the true underlying image.

This confirms that our method scales well to high-dimensional scientific inverse tasks.

Table 2. Peak signal-to-noise ratio (PSNR, higher is better) on 100 black hole imaging tasks. Standard deviations over tasks in parentheses.

Methods	PSNR (\uparrow)
<i>Traditional Methods</i>	
SMILI (Chandra et al., 2018)	22.67 (3.13)
EHT-Imaging (Chael et al., 2018)	24.28 (3.63)
<i>Test-time Guidance Methods</i>	
CBG (gradient-free, ours)	26.10 (3.83)
DPS (Chung et al., 2023)	25.86 (3.90)
LGD (Song et al., 2023b)	21.22 (3.64)
RED-diff (Mardani et al., 2024)	23.77 (4.13)
PnP-DM (Wu et al., 2024)	26.07 (3.70)
DAPS (Zhang et al., 2024)	25.60 (3.64)
DiffPIR (Zhu et al., 2023)	25.01 (4.64)

7. Conclusion

In this work, we address an important gap in the literature of test-time guidance for diffusion models: The common approximations for the diffused likelihoods as well as gradient rescaling are biased, which prevents sampling from the true Bayesian posterior. This does not pose problems for some applications: For natural image inverse synthesis, we usually care more about maximal adherence to the likelihood and image quality rather than calibrated inference in a Bayesian sense. But we argue that for scientific scenarios, proper uncertainty calibration is essential.

We propose two novel estimators that allow to arbitrarily reduce this bias by leveraging the strong signal from evaluating the likelihood function on actual diffusion samples. By increasing computational resources, this converges to the true Bayesian posterior. The gradient-free estimator is particularly easy to adapt to new scenarios as it does not require computing likelihood and diffusion model gradients.

Limitations. The reduced bias comes with a cost: Our estimators require samples from $p(x | x_t)$, which can be expensive. Given the progress in few-step diffusion models (Song et al., 2023c; Geng et al., 2025; Frans et al., 2025), this could be addressed by pretraining models that generate samples from $p(x | x_t)$ in one function call.

Acknowledgements

Stephan Mandt acknowledges funding from the National Science Foundation (NSF) through an NSF CAREER Award IIS-2047418, IIS-2007719, the NSF LEAP Center, and the Hasso Plattner Research Center at UCI, and the Chan Zuckerberg Initiative. This project was supported by the Chan Zuckerberg Initiative, and the Hasso Plattner Research Center at UCI.

We thank Kushagra Pandey and Justus Will for their valuable feedback on the manuscript.

Impact Statement

This paper presents work whose goal is to advance the field of Machine Learning. There are many potential societal consequences of our work, none which we feel must be specifically highlighted here.

References

Albergo, M. S. and Vanden-Eijnden, E. Building normalizing flows with stochastic interpolants. In *The Eleventh International Conference on Learning Representations*, 2023. URL <https://openreview.net/forum?id=li7qeBbCR1t>.

Arfken, G. B., Weber, H. J., and Harris, F. E. *Mathematical methods for physicists: a comprehensive guide*. Academic press, 2011.

Bansal, A., Chu, H.-M., Schwarzschild, A., Sengupta, R., Goldblum, M., Geiping, J., and Goldstein, T. Universal guidance for diffusion models. In *The Twelfth International Conference on Learning Representations*, 2024. URL <https://openreview.net/forum?id=pzpwBbnwiJ>.

Beaumont, M. A., Cornuet, J.-M., Marin, J.-M., and Robert, C. P. Adaptive approximate bayesian computation. *Biometrika*, 96(4):983–990, 2009. ISSN 00063444, 14643510. URL <http://www.jstor.org/stable/27798882>.

Black, K., Janner, M., Du, Y., Kostrikov, I., and Levine, S. Training diffusion models with reinforcement learning. In *The Twelfth International Conference on Learning*

Representations, 2024. URL <https://openreview.net/forum?id=YCWjhGrJFD>.

Chael, A. A., Johnson, M. D., Bouman, K. L., Blackburn, L. L., Akiyama, K., and Narayan, R. Interferometric imaging directly with closure phases and closure amplitudes. *The Astrophysical Journal*, 857(1):23, 2018.

Chandra, S., Dowling, J., Engstrom, C., Xia, Y., Paproki, A., Neubert, A., Rivest-Hénault, D., Salvado, O., Crozier, S., and Fripp, J. A simple framework for the rapid development of biomedical imaging applications. *Computer Methods and Programs in Biomedicine*, 2018.

Chung, H., Sim, B., Ryu, D., and Ye, J. C. Improving diffusion models for inverse problems using manifold constraints. In Oh, A. H., Agarwal, A., Belgrave, D., and Cho, K. (eds.), *Advances in Neural Information Processing Systems*, 2022a. URL <https://openreview.net/forum?id=nJJjv0JDJju>.

Chung, H., Sim, B., and Ye, J. C. Come-closer-diffuse-faster: Accelerating conditional diffusion models for inverse problems through stochastic contraction. In *Proceedings of the IEEE/CVF conference on computer vision and pattern recognition*, pp. 12413–12422, 2022b.

Chung, H., Kim, J., McCann, M. T., Klasky, M. L., and Ye, J. C. Diffusion posterior sampling for general noisy inverse problems. In *The Eleventh International Conference on Learning Representations*, 2023. URL <https://openreview.net/forum?id=OnD9zGAGT0k>.

Corso, G., Stärk, H., Jing, B., Barzilay, R., and Jaakkola, T. S. Diffdock: Diffusion steps, twists, and turns for molecular docking. In *The Eleventh International Conference on Learning Representations*, 2023. URL https://openreview.net/forum?id=kKF8_K-mBbS.

Dhariwal, P. and Nichol, A. Q. Diffusion models beat GANs on image synthesis. In Beygelzimer, A., Dauphin, Y., Liang, P., and Vaughan, J. W. (eds.), *Advances in Neural Information Processing Systems*, 2021. URL <https://openreview.net/forum?id=AAWuCVzaVt>.

Fan, Y., Watkins, O., Du, Y., Liu, H., Ryu, M., Boutilier, C., Abbeel, P., Ghavamzadeh, M., Lee, K., and Lee, K. Reinforcement learning for fine-tuning text-to-image diffusion models. In *Thirty-seventh Conference on Neural Information Processing Systems*, 2023. URL <https://openreview.net/forum?id=80TPepXzeh>.

Frans, K., Hafner, D., Levine, S., and Abbeel, P. One step diffusion via shortcut models. In *The Thirteenth International Conference on Learning Representations*, 2025. URL <https://openreview.net/forum?id=0lzB6LnXcS>.

- Friedman, J. On multivariate goodness-of-fit and two-sample testing. *Conference on Statistical Problems in Particle Physics, Astrophysics and Cosmology*, 2004.
- Friel, N. and Pettitt, A. N. Marginal likelihood estimation via power posteriors. *Journal of the Royal Statistical Society Series B: Statistical Methodology*, 70(3):589–607, 2008.
- Geng, Z., Deng, M., Bai, X., Kolter, J. Z., and He, K. Mean flows for one-step generative modeling. In *The Thirtieth Annual Conference on Neural Information Processing Systems*, 2025. URL <https://openreview.net/forum?id=uWj4s7rMnR>.
- Greenberg, D., Nonnenmacher, M., and Macke, J. H. Automatic posterior transformation for likelihood-free inference. In *Proceedings of the 36th International Conference on Machine Learning*, volume 97 of *Proceedings of Machine Learning Research*, pp. 2404–2414. PMLR, 2019.
- He, Y., Murata, N., Lai, C.-H., Takida, Y., Uesaka, T., Kim, D., Liao, W.-H., Mitsufuji, Y., Kolter, J. Z., Salakhutdinov, R., and Ermon, S. Manifold preserving guided diffusion. In *The Twelfth International Conference on Learning Representations*, 2024. URL <https://openreview.net/forum?id=o3BxOLOxml>.
- Hermans, J., Begy, V., and Louppe, G. Likelihood-free MCMC with approximate likelihood ratios. In *Proceedings of the 37th International Conference on Machine Learning*, volume 98 of *Proceedings of Machine Learning Research*. PMLR, 2020.
- Ho, J. and Salimans, T. Classifier-free diffusion guidance. In *NeurIPS 2021 Workshop on Deep Generative Models and Downstream Applications*, 2021. URL <https://openreview.net/forum?id=qw8AKxfYbI>.
- Ho, J., Jain, A., and Abbeel, P. Denoising diffusion probabilistic models. *Advances in neural information processing systems*, 33:6840–6851, 2020.
- Ho, J., Salimans, T., Gritsenko, A., Chan, W., Norouzi, M., and Fleet, D. J. Video diffusion models. *Advances in neural information processing systems*, 35:8633–8646, 2022.
- Hoogeboom, E., Satorras, V. G., Vignac, C., and Welling, M. Equivariant diffusion for molecule generation in 3d. In *International conference on machine learning*, pp. 8867–8887. PMLR, 2022.
- Huang, Y., Ghatare, A., Liu, Y., Hu, Z., Zhang, Q., Chandra, S., Gururani, S., Oore, S., and Yue, Y. Symbolic music generation with non-differentiable rule guided diffusion. In *Proceedings of the 41st International Conference on Machine Learning*, volume 235, 2024.
- Janati, Y., MOUFAD, B., Durmus, A. O., Moulines, E., and Olsson, J. Divide-and-conquer posterior sampling for denoising diffusion priors. In *The Thirty-eighth Annual Conference on Neural Information Processing Systems*, 2024. URL <https://openreview.net/forum?id=BOrut7M2X7>.
- Jazbec, M., Wong-Toi, E., Xia, G., Zhang, D., Nalisnick, E., and Mandt, S. Generative uncertainty in diffusion models. In Chiappa, S. and Magliacane, S. (eds.), *Proceedings of the Forty-first Conference on Uncertainty in Artificial Intelligence*, volume 286 of *Proceedings of Machine Learning Research*, pp. 1837–1858. PMLR, 21–25 Jul 2025. URL <https://proceedings.mlr.press/v286/jazbec25a.html>.
- Kadkhodaie, Z. and Simoncelli, E. P. Stochastic solutions for linear inverse problems using the prior implicit in a denoiser. In Beygelzimer, A., Dauphin, Y., Liang, P., and Vaughan, J. W. (eds.), *Advances in Neural Information Processing Systems*, 2021. URL <https://openreview.net/forum?id=x5hh6N9bUUb>.
- Karras, T., Aittala, M., Aila, T., and Laine, S. Elucidating the design space of diffusion-based generative models. *Advances in neural information processing systems*, 35:26565–26577, 2022.
- Kawar, B., Elad, M., Ermon, S., and Song, J. Denoising diffusion restoration models. In *Advances in Neural Information Processing Systems*, 2022.
- Li, X., Zhao, Y., Wang, C., Scalia, G., Eraslan, G., Nair, S., Biancalani, T., Regev, A., Levine, S., and Uehara, M. Derivative-free guidance in continuous and discrete diffusion models with soft value-based decoding. *arXiv preprint arXiv:2408.08252*, 2024.
- Lipman, Y., Chen, R. T. Q., Ben-Hamu, H., Nickel, M., and Le, M. Flow matching for generative modeling. In *The Eleventh International Conference on Learning Representations*, 2023. URL <https://openreview.net/forum?id=PqvMRDCJT9t>.
- Liu, X., Gong, C., and qiang liu. Flow straight and fast: Learning to generate and transfer data with rectified flow. In *The Eleventh International Conference on Learning Representations*, 2023. URL <https://openreview.net/forum?id=XVjTT1nw5z>.
- Lueckmann, J.-M., Boelts, J., Greenberg, D., Goncalves, P., and Macke, J. Benchmarking simulation-based inference. In *Proceedings of The 24th International Conference on Artificial Intelligence and Statistics*, volume 130 of *Proceedings of Machine Learning Research*, pp. 343–351, 13–15 Apr 2021.

- Mandt, S., McInerney, J., Abrol, F., Ranganath, R., and Blei, D. Variational tempering. In *Proceedings of the 19th International Conference on Artificial Intelligence and Statistics*, 2016. URL <https://proceedings.mlr.press/v51/mandt16.pdf>.
- Mardani, M., Song, J., Kautz, J., and Vahdat, A. A variational perspective on solving inverse problems with diffusion models. *ICLR*, 2024.
- Miller, A., Foti, N., D’Amour, A., and Adams, R. P. Reducing reparameterization gradient variance. *Advances in Neural Information Processing Systems*, 30, 2017.
- Mizuno, Y. Grmhd simulations and modeling for jet formation and acceleration region in agns. *Universe*, 8(2): 85, January 2022. ISSN 2218-1997. doi: 10.3390/universe8020085. URL <http://dx.doi.org/10.3390/universe8020085>.
- Paisley, J., Blei, D. M., and Jordan, M. I. Variational bayesian inference with stochastic search. In *International Conference on Machine Learning*, 2012.
- Pandey, K., Yang, R., and Mandt, S. Fast samplers for inverse problems in iterative refinement models. In *The Thirty-eighth Annual Conference on Neural Information Processing Systems*, 2024. URL <https://openreview.net/forum?id=qxS4IvtLdD>.
- Pandey, K., Pathak, J., Xu, Y., Mandt, S., Pritchard, M., Vahdat, A., and Mardani, M. Heavy-tailed diffusion models. In *The Thirteenth International Conference on Learning Representations*, 2025a. URL <https://openreview.net/forum?id=toz1OEN4qp>.
- Pandey, K., Sofian, F. M., Draxler, F., Karaletsos, T., and Mandt, S. Variational control for guidance in diffusion models. In *Forty-second International Conference on Machine Learning*, 2025b. URL <https://openreview.net/forum?id=Z0ffRRtOim>.
- Papamakarios, G. and Murray, I. Fast ϵ -free inference of simulation models with Bayesian conditional density estimation. In *Advances in Neural Information Processing Systems 29*, pp. 1028–1036. Curran Associates, Inc., 2016.
- Papamakarios, G., Sterratt, D., and Murray, I. Sequential neural likelihood: Fast likelihood-free inference with autoregressive flows. In *Proceedings of the 22nd International Conference on Artificial Intelligence and Statistics (AISTATS)*, volume 89 of *Proceedings of Machine Learning Research*, pp. 837–848. PMLR, 2019.
- Pawlowski, J. M., Stamatescu, I.-O., and Ziegler, F. P. Cooling stochastic quantization with colored noise. *Physical Review D*, 96(11), December 2017. ISSN 2470-0029. doi: 10.1103/physrevd.96.114505. URL <http://dx.doi.org/10.1103/PhysRevD.96.114505>.
- Potapchik, P., Saravanan, A., Mammadov, A., Prat, A., Albergio, M. S., and Teh, Y. W. Meta flow maps enable scalable reward alignment. *arXiv preprint arXiv:2601.14430*, 2026.
- Pritchard, J. K., Seielstad, M. T., Perez-Lezaun, A., and Feldman, M. W. Population growth of human y chromosomes: a study of y chromosome microsatellites. *Molecular Biology and Evolution*, 16(12):1791–1798, 1999.
- Rockafellar, R. T. *Convex analysis*. Princeton Landmarks in Mathematics and Physics. Princeton University Press, Princeton, NJ, December 1996.
- Rombach, R., Blattmann, A., Lorenz, D., Esser, P., and Ommer, B. High-resolution image synthesis with latent diffusion models. In *Proceedings of the IEEE/CVF conference on computer vision and pattern recognition*, pp. 10684–10695, 2022.
- Ruiz, F. R., Titsias RC AUEB, M., and Blei, D. The generalized reparameterization gradient. In Lee, D., Sugiyama, M., Luxburg, U., Guyon, I., and Garnett, R. (eds.), *Advances in Neural Information Processing Systems*, volume 29. Curran Associates, Inc., 2016. URL https://proceedings.neurips.cc/paper_files/paper/2016/file/f718499c1c8cef6730f9fd03c8125cab-Paper.pdf.
- Sohl-Dickstein, J., Weiss, E., Maheswaranathan, N., and Ganguli, S. Deep unsupervised learning using nonequilibrium thermodynamics. In *International conference on machine learning*, pp. 2256–2265. pmlr, 2015.
- Song, J., Vahdat, A., Mardani, M., and Kautz, J. Pseudoinverse-guided diffusion models for inverse problems. In *International Conference on Learning Representations*, 2023a. URL https://openreview.net/forum?id=9_gsMA8MRKQ.
- Song, J., Zhang, Q., Yin, H., Mardani, M., Liu, M.-Y., Kautz, J., Chen, Y., and Vahdat, A. Loss-guided diffusion models for plug-and-play controllable generation. In *Proceedings of the 40th International Conference on Machine Learning*, volume 202 of *Proceedings of Machine Learning Research*, pp. 32483–32498. PMLR, 23–29 Jul 2023b. URL <https://proceedings.mlr.press/v202/song23k.html>.
- Song, Y. and Ermon, S. Generative modeling by estimating gradients of the data distribution. *Advances in neural information processing systems*, 32, 2019.

- Song, Y., Sohl-Dickstein, J., Kingma, D. P., Kumar, A., Ermon, S., and Poole, B. Score-based generative modeling through stochastic differential equations. In *International Conference on Learning Representations*, 2021. URL <https://openreview.net/forum?id=PxtTIG12RRHS>.
- Song, Y., Dhariwal, P., Chen, M., and Sutskever, I. Consistency models. In Krause, A., Brunskill, E., Cho, K., Engelhardt, B., Sabato, S., and Scarlett, J. (eds.), *Proceedings of the 40th International Conference on Machine Learning*, volume 202 of *Proceedings of Machine Learning Research*, pp. 32211–32252. PMLR, 23–29 Jul 2023c. URL <https://proceedings.mlr.press/v202/song23a.html>.
- Tang, H., Xie, T., Feng, A., Wang, H., Zhang, C., and Bai, Y. Solving noisy inverse problems via posterior sampling: A policy gradient view-point. In *The Symbiosis of Deep Learning and Differential Equations III*, 2023.
- Uehara, M., Zhao, Y., Black, K., Hajiramezanali, E., Scalia, G., Diamant, N. L., Tseng, A. M., Biancalani, T., and Levine, S. Fine-tuning of continuous-time diffusion models as entropy-regularized control. *arXiv preprint arXiv:2402.15194*, 2024.
- Williams, R. J. Simple statistical gradient-following algorithms for connectionist reinforcement learning. *Mach. Learn.*, 8(3-4):229–256, May 1992.
- Wu, Z., Sun, Y., Chen, Y., Zhang, B., Yue, Y., and Bouman, K. Principled probabilistic imaging using diffusion models as plug-and-play priors. In *The Thirty-eighth Annual Conference on Neural Information Processing Systems*, 2024. URL <https://openreview.net/forum?id=Xq9HQf7VNV>.
- Wuttke, R., Hofmann, H., Nettels, D., Borgia, M. B., Mittal, J., Best, R. B., and Schuler, B. Temperature-dependent solvation modulates the dimensions of disordered proteins. *Proceedings of the National Academy of Sciences*, 111(14):5213–5218, 2014.
- Yang, R., Srivastava, P., and Mandt, S. Diffusion probabilistic modeling for video generation. *Entropy*, 25(10):1469, 2023.
- Ye, H., Lin, H., Han, J., Xu, M., Liu, S., Liang, Y., Ma, J., Zou, J., and Ermon, S. TFG: Unified training-free guidance for diffusion models. In *The Thirty-eighth Annual Conference on Neural Information Processing Systems*, 2024. URL <https://openreview.net/forum?id=N8YbGX98vc>.
- Yu, J., Wang, Y., Zhao, C., Ghanem, B., and Zhang, J. Freedom: Training-free energy-guided conditional diffusion model. In *Proceedings of the IEEE/CVF International Conference on Computer Vision*, pp. 23174–23184, 2023.
- Zhang, B., Chu, W., Berner, J., Meng, C., Anandkumar, A., and Song, Y. Improving diffusion inverse problem solving with decoupled noise annealing, 2024. URL <https://arxiv.org/abs/2407.01521>.
- Zheng, H., Chu, W., Zhang, B., Wu, Z., Wang, A., Feng, B., Zou, C., Sun, Y., Kovachki, N. B., Ross, Z. E., Bouman, K., and Yue, Y. Inversebench: Benchmarking plug-and-play diffusion priors for inverse problems in physical sciences. In *The Thirteenth International Conference on Learning Representations*, 2025. URL <https://openreview.net/forum?id=U3PBITXNG6>.
- Zhu, Y., Zhang, K., Liang, J., Cao, J., Wen, B., Timofte, R., and Gool, L. V. Denoising diffusion models for plug-and-play image restoration. In *IEEE Conference on Computer Vision and Pattern Recognition Workshops (NTIRE)*, 2023.

A. Proofs

A.1. Proof for Theorem 4.1

Proof. The forward direction is simple: If the likelihood $p(y | x)$ is constant in x , then

$$p(y | x_t) = \int p(x | x_t)p(y | x)dx = \int p(x | x_t)p(y | x = 0)dx = p(y | x = 0) \int p(x | x_t)dx = p(y | x = 0). \quad (23)$$

For the reverse direction, we assume $t \ll 1$, that is we are close to the data distribution. Given that $p(x)$ is Lipschitz, there exists $t > 0$ so that:

$$p(x | x_t) \approx \mathcal{N}(\hat{x}_t, \Sigma_t), \quad \text{where } \Sigma_t = \text{Cov}[x | x_t]. \quad (24)$$

The covariance Σ_t is positive definite because $p(x)$ is continuous (through Lipschitz) and so has nonzero support in all directions.

Now let us expand $p(y | x_t)$ around the posterior mean $\hat{x}(x_t) = \mathbb{E}[x | x_t]$:

$$p(y | x_t) = \mathbb{E}[p(y | x) | x_t] = p(y | x = \hat{x}(x_t)) + \frac{1}{2} \text{tr}(\Sigma_t \nabla^2 p(y | x = \hat{x}(x_t))) + O(\sigma_t^3). \quad (25)$$

Here, $\nabla^2 p(y | x = \hat{x}(x_t))$ is the Hessian of the likelihood function. By assumption, it holds that:

$$p(y | x_t) = p(y | x = \hat{x}(x_t)). \quad (26)$$

Comparing the two equations, we find that the second derivative of $p(y | x)$ is zero everywhere, implying that it is an affine function. However, also by assumption $p(y | x)$ is nonnegative, and affine functions can only be nonnegative if they are constant. □

On the regularity assumptions: The Lipschitz assumption excludes the case of discontinuities in the distribution, allowing the Gaussian approximation and positive definite posterior covariance; in practice, one can approximate distributions with hard jumps by distributions with strong but bounded gradients, with vanishing effect on the result. Note that in particular this is no restriction on the tail behavior of the distribution.

A.2. Proof for Theorem 4.2

Proof. Write $q(x) = \mathcal{N}(x; 0, I)$ for the standard normal. Inserting $p(x) = q(x)$ on the left hand side of Equation (8) establishes that both sides are identical for all x_t , as then $p(x | x_t) = \mathcal{N}(x; \mathbb{E}[x | x_t], \sigma_t^2 I)$. This trivially implies following identity (via Bayes' theorem):

$$\frac{\int p(x)p(x_t | x)p(y | x)dx}{\int p(x')p(x_t | x')dx'} = \frac{\int q(x)p(x_t | x)p(y | x)dx}{\int q(x')p(x_t | x')dx'}, \quad \forall x_t. \quad (27)$$

We now assume that Equation (27) holds, but $p(x)$ is not a standard normal. We will follow that either $p(x)$ is Gaussian (a contradiction, proving that the only $p(x)$ for which Equation (8) is accurate is a standard normal prior) or $p(y | x)$ is constant in x (which we excluded).

Throughout this proof, for notational simplicity, we ignore the dependence of the likelihood $p(y | x)$ on the constant y , and write $f(x) = p(y | x)$.

Cross-multiplying the denominators in Equation (27):

$$\int p(x)p(x_t | x)f(x)dx \int q(x')p(x_t | x')dx' - \int q(x)p(x_t | x)f(x)dx \int p(x')p(x_t | x')dx', \quad \forall x_t. \quad (28)$$

Combine into one double integral:

$$\iint [p(x)q(x') - q(x)p(x')]f(x)p(x_t | x)p(x_t | x')dx dx' = 0, \quad \forall x_t. \quad (29)$$

Now, note that $p(x)q(x') - q(x)p(x')$ is antisymmetric under swapping under the exchange $x \leftrightarrow x'$, while $p(x_t | x)p(x_t | x')$ is symmetric. Swapping $x \leftrightarrow x'$, we find:

$$\iint [p(x')q(x) - q(x')p(x)]f(x')p(x_t | x)p(x_t | x')dx dx' = 0, \quad \forall x_t. \quad (30)$$

Subtracting the second variant of this integral from the first, we find:

$$\iint [p(x)q(x') - q(x)p(x')][f(x) - f(x')]p(x_t | x)p(x_t | x')dx dx' = 0, \quad \forall x_t. \quad (31)$$

Define:

$$H(x, x') = [p(x)q(x') - q(x)p(x')][f(x) - f(x')]. \quad (32)$$

Substitute $u = a_t x, v = a_t x'$, and write $\tilde{H}(u, v) = a_t^{-2d} H(u/a_t, v/a_t)$. This is possible because $a_t > 0$ by $t < 1$. Then, we have that:

$$\iint \tilde{H}(u, v)\varphi_{b_t}(x_t - u)\varphi_{b_t}(x_t - v)dudv = 0, \quad \forall x_t. \quad (33)$$

Here, by $\varphi_\sigma(z) = \mathcal{N}(z, 0, \sigma^2 I)$ is the centered isotropic Gaussian with variance σ^2 . It holds that $\sigma > 0$ because $0 < t$.

Again substitute, now with $w = (u + v)/2$ and $z = u - v$ (which means that $u = w + z/2, v = w - z/2$, with unit Jacobian determinant). It is easy to confirm that the product of Gaussians factorizes in terms of w and z :

$$\varphi_{b_t}(x_t - u)\varphi_{b_t}(x_t - v) = C_d \varphi_{b_t/\sqrt{2}}(x_t - w)\varphi_{b_t\sqrt{2}}(z). \quad (34)$$

The constant $C_d = (2\pi b_t^2)^{-d/2}$ arises from reconciling normalizations. Writing $\tilde{\tilde{H}}(w, z) = \tilde{H}(w + z/2, w - z/2)$, we find:

$$C_d \int \left[\int \tilde{\tilde{H}}(w, z)\varphi_{b_t\sqrt{2}}(z)dz \right] \varphi_{b_t/\sqrt{2}}(x_t - w)dw = 0, \quad \forall x_t. \quad (35)$$

Per Lemma A.1 with the inner integral as test function, this implies that:

$$\int \tilde{\tilde{H}}(w, z)\varphi_{b_t\sqrt{2}}(z)dz = 0, \quad \forall w. \quad (36)$$

Applying the same Lemma A.1 again, we find that:

$$\tilde{\tilde{H}}(w, z) = \tilde{H}(w + z/2, w - z/2) = 0, \quad \forall w, z. \quad (37)$$

In turn, this means that:

$$[p(x)q(x') - q(x)p(x')][f(x) - f(x')] = 0, \quad \forall x, x'. \quad (38)$$

Defining the density ratio $r(x) = p(x)/q(x)$ (well-defined since $q(x) > 0$), Equation (38) becomes (divide by $q(x)q(x')$):

$$[r(x) - r(x')][f(x) - f(x')] = 0, \quad \forall x, x'. \quad (39)$$

Thus, by Lemma A.2, at least one of f or r must be constant.

Going back to the beginning of the proof, Equation (8) is correct if at least one of the following statements is true:

- $f(x) = \text{const}$, which is the trivial case in which $p(x)$ can be arbitrary as we apply no guidance. We excluded this case in the statement.
- $r(x) = \text{const}$, which implies $p(x) = q(x) = \mathcal{N}(x; 0, I)$ (since they are both normalized to 1). This contradicts the earlier assumption that $p(x)$ is not Gaussian. Therefore Equation (27) cannot be fulfilled for all $x_t \in \mathbb{R}^d$ if $p(x) \neq \mathcal{N}(x; 0, I)$. Therefore, Equation (8) is biased for all $0 < t < 1$.

□

Here, we have used the following results:

Lemma A.1. *Given a function $f : \mathbb{R}^d \rightarrow \mathbb{R}$ and $q(x) = \mathcal{N}(x; 0, \Sigma)$ for some strictly positive definite Σ . If it holds that:*

$$\int f(x)q(x - u)dx = 0, \quad \forall u, \quad (40)$$

then it follows that:

$$f(x) = 0. \quad (41)$$

Proof. Equation (40) has the form of a convolution. By the convolution theorem (Arfken et al., 2011), we have that:

$$\mathcal{F}[f](\xi) \cdot \mathcal{F}[\mathcal{N}(\cdot; 0, \Sigma)](\xi) = 0, \quad \forall \xi. \quad (42)$$

Since $\mathcal{F}[\mathcal{N}(\cdot; 0, \Sigma)](\xi) > 0$ for all ξ , it follows that:

$$\mathcal{F}[f](\xi) = 0, \quad \forall \xi. \quad (43)$$

Therefore,

$$f(x) = 0. \quad (44)$$

□

Lemma A.2. *Given two functions $f, g : \mathbb{R}^d \rightarrow \mathbb{R}$. If it holds that*

$$[f(x) - f(y)][g(x) - g(y)] = 0, \quad \forall x, y \in \mathbb{R}^d, \quad (45)$$

it follows that at least one of f or g is a constant function.

Proof. Without loss of generality, we assume that f is non-constant and show that g is constant.

Take any two points $x, y \in \mathbb{R}^d$.

Case 1: $f(x) \neq f(y)$, Equation (45) immediately shows that $g(x) = g(y)$.

Case 2: $f(x) = f(y)$, take a third point $z \in \mathbb{R}^d$ for which $f(z) \neq f(x)$. It follows that $g(x) = g(z)$ by the same argument. What does this reveal about $g(y)$?

Case 2a: $f(z) = f(y)$. However, per $f(x) = f(y)$ this would imply that $f(x) = f(z)$, which contradicts how we chose z . This case is therefore never achieved.

Case 2b: $f(z) \neq f(y)$. Therefore, $g(z) = g(y)$ by the first argument. □

A.3. Proof for Theorem 4.3

Proof. The function $f(x) = x^\gamma$ is concave for $\gamma \in (0, 1)$, and convex for $\gamma > 1$.

Therefore, for $0 < \gamma \neq 1$, equality in

$$\int p(x | x_t)p(y | x)^\gamma dx = \left(\int p(x | x_t)p(y | x) dx \right)^\gamma \quad (46)$$

holds if and only if $p(y | x)$ is an affine function by Lemma A.3. Per the same argument as in the proof of Theorem 4.1, $p(y | x)$ can only be constant. □

Lemma A.3. *Given a function $f(x)$ that is either concave or convex but not strictly so. Then, for any probability distribution $p(x)$, it holds that:*

$$\int p(x)f(x)dx = f(\mathbb{E}_{x \sim p(x)}[x]) \quad \text{if and only if} \quad f(x) = a^T x + b \quad p(x)\text{-almost surely.} \quad (47)$$

Proof. By (Rockafellar, 1996), Jensen’s inequality states for a convex f :

$$\int p(x)f(x)dx \geq f(\mathbb{E}_{x \sim p(x)}[x]). \quad (48)$$

The reverse inequality holds for concave f :

$$\int p(x)f(x)dx \leq f(\mathbb{E}_{x \sim p(x)}[x]). \quad (49)$$

Only for a concave *and* convex function, both equalities hold. This is the case where f is affine ($p(x)$ -almost surely; that is there are only sets of measure zero where the function deviates from the global affine function). \square

B. Algorithm

Algorithm 1 Calibrated Bayesian Guidance

Input: Initial noise $x_T \sim \mathcal{N}(0, 1)$
for $t = T$ **to** 1 **do**
 Draw samples from $p(x | x_t)$
 Compute $\nabla_{x_t} \log p(x_t | y)$ with Equations (5) and (16) or Equation (20)
 Compute x_{t-1} with an Euler step along Equation (2)
end for

C. Gradient-free and Gradient-based Methods

We consider the case where we have a simple prior $p(x) = \mathcal{N}(x; 2, 1)$ and a simple likelihood $p(y|x) = \mathcal{N}(y; 0, 0.4^2)$. Denote $\hat{x}(x_t)$ as the exact analytic estimate for $\mathbb{E}[x|x_t, y]$, and $\hat{x}_{\text{grad-free}}(x_t)$, $\hat{x}_{\text{grad-based}}(x_t)$ our estimates from the CBG gradient-free and CBG gradient-based algorithms using Tweedie’s formula. We plot the variances $\mathbb{E} \left[(\hat{x}_{\text{grad-based}}(x_t) - \hat{x}(x_t))^2 \right]$ and $\mathbb{E} \left[(\hat{x}_{\text{grad-free}}(x_t) - \hat{x}(x_t))^2 \right]$ as we vary x_t and t . Both estimators use $K = 1000$ samples, with the variance expectation estimated over 100 algorithm calls. Looking at Figure 5, there is a clear region to the left of $t \approx 0.3$ where gradient-based method performs better, but noticeably not by much.

D. Bayesian Inference Benchmark Guidance Methods

D.1. Diffusion Process

For all guidance methods, the flow matching forward process was used:

$$p(x_t|x) = \mathcal{N}(x_t; (1-t)x, t^2I)$$

For generation, t is scheduled to linearly decrease from 1 to 0.

D.2. Diffusion Posterior Sampling

Diffusion Posterior Sampling (DPS) (Chung et al., 2023) approximates the score $\nabla_{x_t} \log p(y|x_t)$ as

$$\nabla_{x_t} \log p(y|x_t) \approx \nabla_{x_t} \log p(y|\mathbb{E}[x|x_t])$$

D.3. Loss Guided Diffusion

Loss Guided Diffusion (LGD) (Song et al., 2023b) approximates the score $\nabla_{x_t} \log p(y|x_t)$ as

$$\nabla_{x_t} \log p(y|x_t) \approx \nabla_{x_t} \log \int p(y|x)q(x|x_t)dx$$

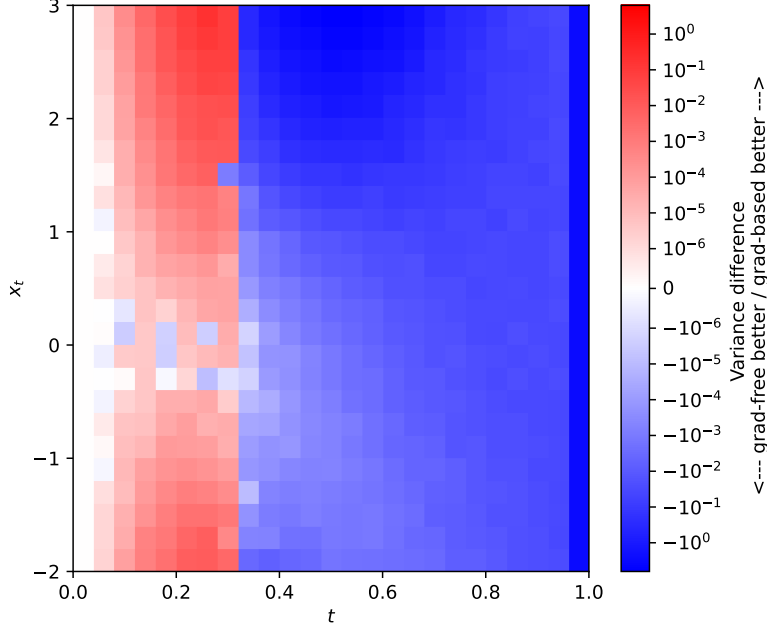


Figure 5. Variance comparison for gradient-free and gradient-based methods. In some regions, the gradient-based method has lower variance.

where $q(x|x_t) = \mathcal{N}\left(\mathbb{E}[x|x_t], \frac{t^2}{(1-t)^2+t^2}I\right)$ approximates the true diffusion posterior distribution. Evaluated using a finite set of samples $x^{(i)} \sim q(x|x_t)$ for $i = 1, \dots, K$, we have:

$$\nabla_{x_t} \log p(y|x_t) \approx \nabla_{x_t} \log \left[\frac{1}{K} \sum_i p(y|x^{(i)}) \right]$$

D.4. Diffusion Policy Gradient

Diffusion Policy Gradient (DPG) (Tang et al., 2023) approximates the score $\nabla_{x_t} \log p(y|x_t)$ as

$$\nabla_{x_t} \log p(y|x_t) \approx C \frac{s(x_t)}{\|s(x_t)\|_2^2}$$

Thus:

$$s(x_t) = \mathbb{E}_{x \sim q(x|x_t)} [(p(y|x) - b) \nabla_{x_t} (-\|x - \mathbb{E}[x|x_t]\|_2^2)]$$

where $q(x|x_t) = \mathcal{N}\left(\mathbb{E}[x|x_t], \frac{t^2}{(1-t)^2+t^2}I\right)$ approximates the true diffusion posterior distribution. Evaluated using a finite set of samples $x^{(i)} \sim q(x|x_t)$ for $i = 1, \dots, K$, we approximate as:

$$s(x_t) \approx \frac{1}{K} \sum_i (p(y|x^{(i)}) - b^{(i)}) \nabla_{x_t} (-\|x^{(i)} - \mathbb{E}[x|x_t]\|_2^2)$$

where $b^{(i)}$ is computed as

$$b^{(i)} = \frac{1}{K-1} \sum_{j=1, j \neq i}^K p(y|x^{(j)})$$

D.5. Stochastic Control Guidance

Stochastic Control Guidance (SCG) (Huang et al., 2024) chooses an $\hat{x}_{t'}$ to transition to, given the current state x_t , as follows:

$$\hat{x}_{t'} = \arg \max_{x_{t'}} p(y|\mathbb{E}[x|x_{t'}])$$

Approximating $p(x_{t'}|x_t)$ as

$$q(x_{t'}|x_t) = \mathcal{N}\left(\frac{t'}{t}x_t + \left(1 - \frac{t'}{t}\right)\mathbb{E}[x|x_t], \sigma^2 I\right), \sigma^2 = \frac{(t-t')^2}{(1-t)^2 + t^2}$$

we can evaluate this using a finite set of samples $x_t^{(i)} \sim q(x|x_t)$ for $i = 1, \dots, K$ as:

$$\hat{x}_{t'} \approx \arg \max_i p\left(y | \mathbb{E}\left[x | x_t^{(i)}\right]\right)$$

E. Bayesian Inference Benchmark Guidance Tasks

E.1. Task 1

Inference on the mean of a 10-dimensional Gaussian, with a Gaussian prior.

Prior: $p(x) = \mathcal{N}(x; 0, 0.1I)$

Diffusion Posterior: $p(x | x_t) = \mathcal{N}\left(x; \frac{1-t}{10t^2+(1-t)^2}x_t, \frac{t^2}{10t^2+(1-t)^2}I\right)$.

Likelihood: $p(y|x) = \mathcal{N}(x; y, 0.1I)$

Dimensionality: $x \in \mathbb{R}^{10}$

E.2. Task 2

Inference on the mean of a 10-dimensional Gaussian, with a uniform prior.

Prior: $p(x) = \mathcal{U}(-1, 1)$

Diffusion Posterior: $p(x | x_t) \propto \mathbf{1}\{x \in [-1, 1]^{10}\} \mathcal{N}\left(x; \frac{x_t}{1-t}, \frac{t^2}{(1-t)^2}I\right)$.

Likelihood: $p(y|x) = \mathcal{N}(y; x, 0.1I)$

Dimensionality: $x \in \mathbb{R}^{10}, y \in \mathbb{R}^{10}$

E.3. Task 3

Inference on the parameters of a 10-dimensional Gaussian with nonlinear mean and variance functions, with a uniform prior.

Prior: $p(x) = \mathcal{U}(-3, 3)$

Diffusion Posterior: $p(x | x_t) \propto \mathbf{1}\{x \in [-3, 3]^5\} \mathcal{N}\left(x; \frac{x_t}{1-t}, \frac{t^2}{(1-t)^2}I\right)$.

Likelihood: $p(y|x) = \prod_{i=1}^4 \mathcal{N}(y^{(i)}; \mu(x), \Sigma(x))$

where $\mu(x) = \begin{bmatrix} x_1 \\ x_2 \end{bmatrix}$, $\Sigma(x) = \begin{bmatrix} s_1^2 & \rho s_1 s_2 \\ \rho s_1 s_2 & s_2^2 \end{bmatrix}$, $s_1 = x_3^2$, $s_2 = x_4^2$, $\rho = \tanh x_5$

Dimensionality: $x \in \mathbb{R}^5, y \in \mathbb{R}^{4 \times 2}$

E.4. Task 4

Inference on the shared mean of a mixture of two 2-dimensional Gaussians, one much broader than the other, with a uniform prior.

Prior: $p(x) = \mathcal{U}(-10, 10)$

Diffusion Posterior: $p(x | x_t) \propto \mathbf{1}\{x \in [-10, 10]^2\} \mathcal{N}\left(x; \frac{x_t}{1-t}, \frac{t^2}{(1-t)^2}I\right)$.

Likelihood: $p(y|x) = 0.5\mathcal{N}(y; x, I) + 0.5\mathcal{N}(y; x, 0.01I)$

Dimensionality: $x \in \mathbb{R}^2, y \in \mathbb{R}^2$

Calibrated Test-Time Guidance for Bayesian Inference

Table 3. Bayesian inference benchmark hyperparameter sweep.

Methods	N	K	γ	C
CBG (gradient-free)	$[10^1, 10^5]$	$[10^1, 10^5]$	N/A	N/A
CBG (gradient-based)	$[10^1, 10^5]$	$[10^1, 10^5]$	N/A	N/A
DPS	$[10^1, 10^5]$	N/A	$[10^{-3}, 10^3]$	N/A
LGD	$[10^1, 10^5]$	$[10^1, 10^5]$	$[10^{-3}, 10^3]$	N/A
DPG	$[10^1, 10^5]$	$[10^1, 10^5]$	$[10^{-3}, 10^3]$	$[10^{-1}, 10^1]$
SCG	$[10^1, 10^5]$	$[10^1, 10^5]$	$[10^{-3}, 10^3]$	N/A

Table 4. Bayesian inference benchmark chosen hyperparameters.

Methods	Task 1				Task 2				Task 3				Task 4				Task 5			
	N	K	γ	C	N	K	γ	C	N	K	γ	C	N	K	γ	C	N	K	γ	C
CBG (grad-free)	100	1000	-	-	100	1000	-	-	100	1000	-	-	100	1000	-	-	100	1000	-	-
CBG (grad-based)	100	1000	-	-	100	1000	-	-	1000	100	-	-	1000	100	-	-	100	1000	-	-
DPS	100	-	0.022	-	100	-	0.022	-	100	-	0.005	-	100	-	0.005	-	10000	-	0.001	-
LGD	100	1000	2.154	-	10	100	10.000	-	10	1000	0.464	-	10	10	0.100	-	10	10000	0.464	-
DPG	10	1000	10.000	10.000	10	1000	2.154	10.000	100	100	0.001	0.100	100	100	0.464	1.000	100	10	215.443	10.000
SCG	10	10	-	-	100	10	-	-	10	100	-	-	10	100	-	-	10	100	-	-

E.5. Task 5

Inference on a two-moons distribution with both bimodality and local structure, with a uniform prior.

Prior: $p(x) = \mathcal{U}(-1, 1)$

Diffusion Posterior: $p(x | x_t) \propto \mathbf{1}\{x \in [-1, 1]^2\} \mathcal{N}\left(x; \frac{x_t}{1-t}, \frac{t^2}{(1-t)^2} I\right)$.

Likelihood: Let $s(x) = \begin{bmatrix} -\frac{|x_1+x_2|}{\sqrt{2}} \\ -\frac{x_1-x_2}{\sqrt{2}} \end{bmatrix}$, $z = y - s(x)$, $u = z_1 - 0.25$, $v = z_2$, $\rho = \sqrt{u^2 + v^2}$, $\phi = \text{atan2}(v, u)$. Then, for $\rho > 0$,

$$p(y | x) = \mathbf{1}\left\{\phi \in \left(-\frac{\pi}{2}, \frac{\pi}{2}\right)\right\} \cdot \frac{1}{\pi \rho} \cdot \frac{\mathcal{N}(\rho; 0.1, 0.01^2)}{\Phi(10)}.$$

F. Experimental Details for Bayesian Inference Benchmark

Table 3 contains the set of hyperparameters tried for all methods, and table 4 contains the chosen hyperparameters to maximize distributional fit. All combinations of hyperparameters were tried, restricting to combinations satisfying $N \cdot K \leq 10^5$, which restricts the total number of likelihood evaluations. CBG does not tune a guidance scale since we aim to sample from the true distribution $p(x|y)$ at $\gamma = 1$. Additionally, some other diffusion models do not use the maximum number of likelihood evaluations since they converge to the wrong distribution, and happen to get better results with less evaluations.

10^4 reference samples are given, and the methods generate 10^4 samples as well.

For experimental details on likelihood-free methods, see [Lueckmann et al. \(2021\)](#).

G. Experimental Details for Black Hole Imaging

We tune hyperparameters on the validation set of InverseBench ([Zheng et al., 2025](#)) dataset. Specifically, the total number of denoising step is fixed to $N = 1000$, while the number of inner-loop steps is selected from the range of $M \in \{25, 50, 100, 1000\}$. The number of samples is chosen from $K \in \{2^5, 2^6, 2^7, 2^8, 2^9, 2^{10}, 2^{11}\}$. Based on validation performance, we select $N = 1000$, $M = 50$, $K = 512$ and $\gamma = 0.003$ for our method, which results in 2h40 per image on a single H100 (note that 80GB of memory are not needed). All experiments are conducted on 100 test samples. For baselines, we adopt the hyperparameter settings reported in Table 12 of the original InverseBench paper to ensure fair comparison.

H. Qualitative Analysis for Black Hole Imaging

See Figures 6 and 7 for several samples for two random black hole imaging tasks.

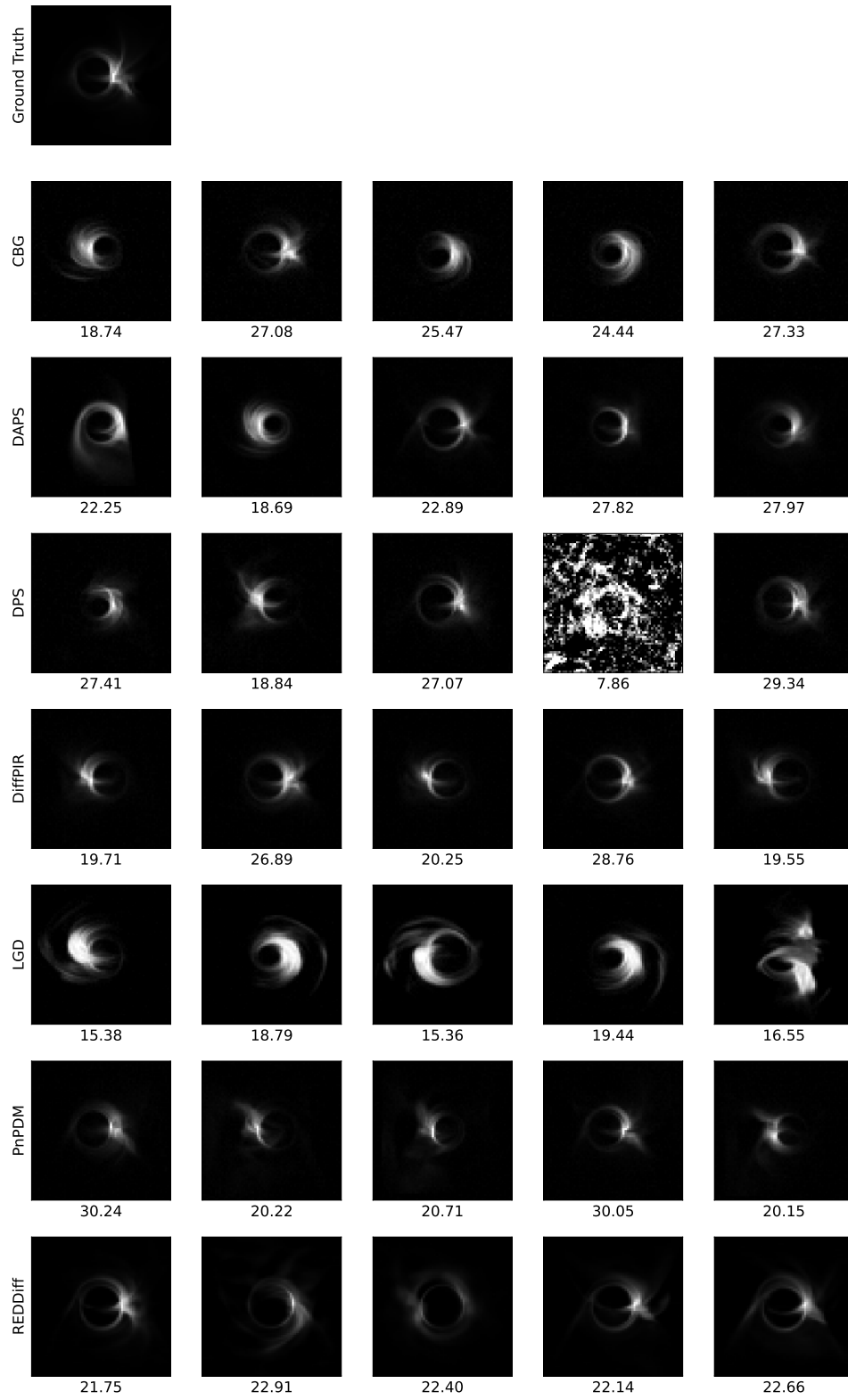


Figure 6. Qualitative analysis of the generative results of the different methods with a random index, five samples were taken per method. The numbers are the PSNR to the ground truth for each task.

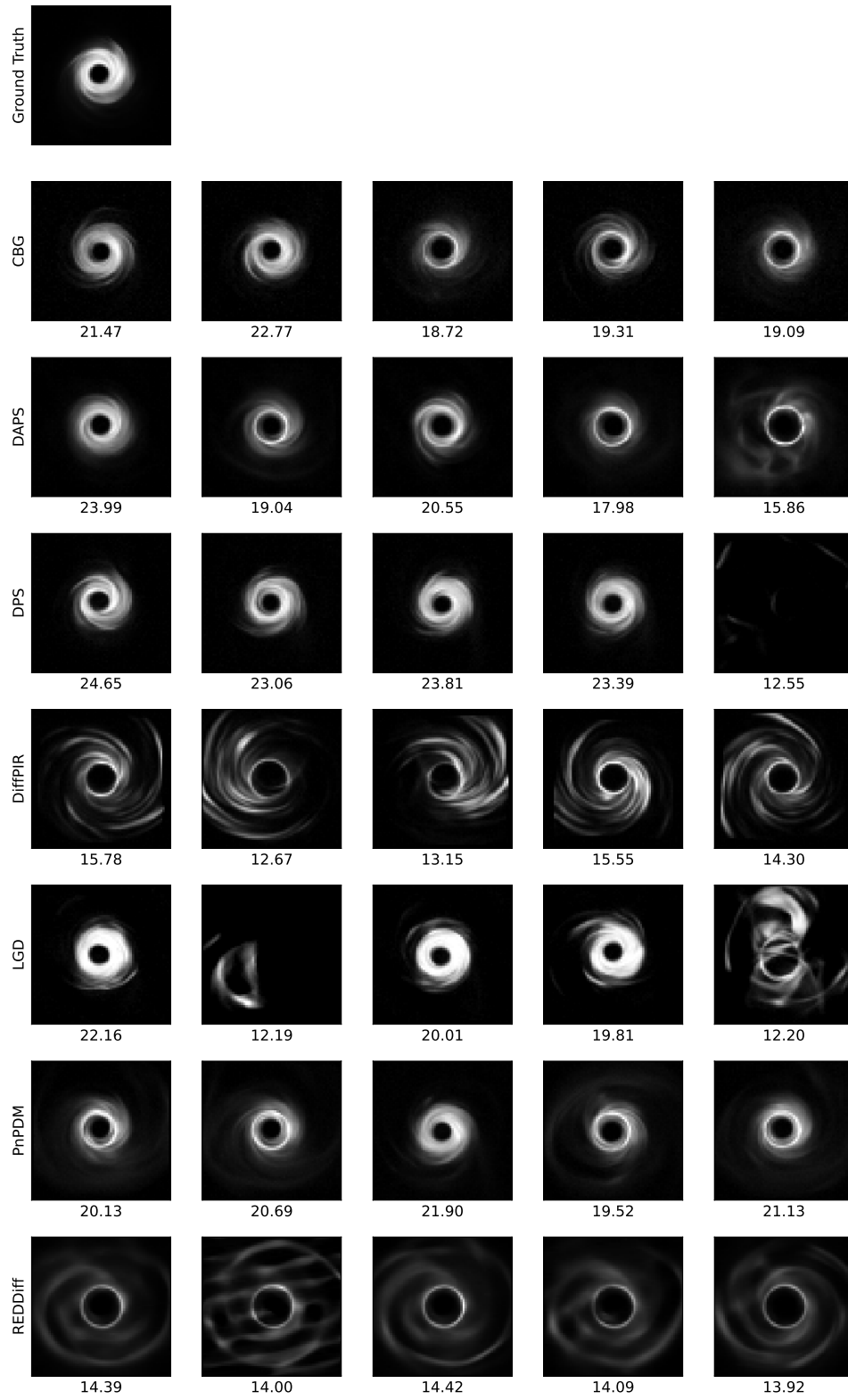


Figure 7. Qualitative analysis of the generative results of the different methods with a different random index, five samples were taken per method. The numbers are the PSNR to the ground truth for each task.